Cell Reports
Physical Science

CellPress
OPEN ACCESS

Article

Natural wood-derived solid ionic conductor for solid electro-Fenton strategy

By creating a natural, wood-derived solid ionic conductor, Cui et al. propose a solid electro-Fenton (EF) strategy to electrochemically produce H_2O_2 and $OH^{\bullet}$ using only water and air. The EF strategy could be used to degrade typical aqueous or gaseous organic pollutants at room temperature.

Jiedong Cui, Yang Li, Chaocheng Liu, Zhiyun Qian, Hui Pan, Detao Liu

dtliu@scut.edu.cn

Highlights

Wood ionic conductor has unique salt-polymer ionic structure for ion transport

The WSIC separates anode and flowable cathodic cell for a solid EF strategy

Solid EF device for cathodic production of H_2O_2 and $OH^{\bullet}$ using air and water

The solid EF strategy degrades typical aqueous and gaseous organic pollutants

Cui et al., Cell Reports Physical Science 3, 100857
May 18, 2022
https://doi.org/10.1016/j.xcrp.2022.100857

Please cite this article in press as: Cui et al., Natural wood-derived solid ionic conductor for solid electro-Fenton strategy, Cell Reports Physical Science (2022), https://doi.org/10.1016/j.xcrp.2022.100857

Cell Reports
Physical Science

CellPress
OPEN ACCESS

Article

Natural wood-derived solid ionic conductor for solid electro-Fenton strategy

Jiedong Cui,[1] Yang Li,[1] Chaocheng Liu,[1] Zhiyun Qian,[1] Hui Pan,[2] and Detao Liu[1,3,*]

SUMMARY

Among the many environmental problems affecting human health and safety, air and water pollution affect millions of people globally. H_2O_2 is a clean oxidant for production of hydroxyl radicals ($OH^{\bullet}$) that decomposes nearly all organic pollutants. However, electro-Fenton (EF) strategies for producing H_2O_2 are still unsatisfactory because of intermittent production, negative decomposition, and the wide use of pure O_2 or/and proton exchange membranes. Here we report a wood-derived solid ionic conductor (WSIC) to propose a solid EF strategy for continuous cathodic production of giant H_2O_2 using only air and water. Effective activation of H_2O_2 by FeOCl generates $OH^{\bullet}$, which continuously degrades aqueous (99.9%, Rhodamine B) or mineralizes gaseous toluene into CO_2 and H_2O at room temperature. Our findings are a fundamental step toward development of next-generation of advanced oxidation processes that are sustainable and cost effective.

INTRODUCTION

Advanced oxidation processes (AOPs) produce highly reactive radicals of hydroxyl radicals ($OH^{\bullet}$), sulfate radicals ($SO_4^{\bullet-}$), and superoxide radicals ($O_2^{\bullet-}$) that can degrade organic pollutants, viruses, and bacteria with a tremendous requirement that has aroused great interest in the global environmental community.[1–7] In most cases, the $OH^{\bullet}$ generated by activating H_2O_2 through the current electro-Fenton, photo-Fenton, and Fenton-like strategies has an extremely high oxidative activity and decomposes nearly all organic pollutants to produce only nontoxic CO_2 and H_2O by-products.[8–11] Despite its ability to remove almost all organic pollutants, conventional Fenton processes still require continuous input of H_2O_2 and Fe^{2+}, making them extremely expensive and complex in large-scale applications.[12–14] The EF strategy derived from the traditional Fenton reaction has become an important technology because of the two-electron reduction of O_2 (2e-ORR) and cathodic regeneration of Fe^{2+} with better controllability, higher efficiency, and environmental compatibility, as described in Equations 1, 2, and 3.[15–17]

$$O_2 + 2H^+ + 2e^- \rightarrow H_2O_2 \quad \text{(Equation 1)}$$

$$H_2O_2 + Fe^{2+} + H^+ \rightarrow Fe^{3+} + OH^{\bullet} + H_2O \quad \text{(Equation 2)}$$

$$Fe^{3+} + e^- \rightarrow Fe^{2+} \quad \text{(Equation 3)}$$

However, for a typical reactor-type EF process, the additional H_2O_2 input is generally replenished in the most practical applications because of the low efficiency, negative H_2O_2 decomposition, and intermittent production of H_2O_2.[18,19] A flowable electro-Fenton (EF) configuration is a promising alternative that can continuously produce higher concentrations of H_2O_2 to meet the requirements of the EF process.

[1]School of Light Industry and Engineering, South China University of Technology, Wushan Rd., 381#, Tianhe District, Guangzhou, Guangdong 510640, China

[2]Institute of Applied Physics and Materials Engineering, University of Macau, Macao SAR 999078, China

[3]Lead contact

*Correspondence: dtliu@scut.edu.cn

https://doi.org/10.1016/j.xcrp.2022.100857

Previous reports have demonstrated that it can increase the decomposition efficiency in an aqueous electrolyte when it allows the aqueous organic contaminants to flow through a cathodic porous carbon nanotube (CNT)-based membrane[20] or a cathodic graphite felt (GF)/carbon cloth.[21] However, the production efficiency of H_2O_2 is still unsatisfactory because of its negative decomposition from anodic oxidation and insufficient mass transfer when assembling them into a whole aqueous electrolyte cell.[22]

The superiority of flowable EF production of H_2O_2 is optimal when we use an ionic conductor as a solid electrolyte to make the separated anode and cathode work together to form a solid EF reactor, avoiding the major concerns of negative secondary decomposition and insufficient mass transfer. However, whether the solid ion electrolyte can work synergistically with the solid EF reaction to boost the final production of H_2O_2 and $OH^{\bullet}$ still remains unknown because of the lack of solid EF reaction mechanisms.

Here we report a wood-derived solid ionic conductor (WSIC) possessing unique ionic transport structures around the abundant, vertically aligned, top-down microchannels that separates the anode and cathodic flow cell to form a solid EF device that electrochemically produces H_2O_2 using only ubiquitous H_2O and air in nature. Cheap commercial GFs are commonly used carbon-based cathode materials in EF systems, possessing high electrical conductivity and high specific surface area.[23–25] Its unique 3D fibrous porous structure is suited for the characteristics of flowable degradation of the designed cathode flow cell. Therefore, the cathodic flow cell is filled completely with a porous untreated commercial GF matrix, offering a sufficient gas-liquid-solid three-phase interface to enhance the oxygen transfer efficiency, andthus, H_2O_2 production efficiency. The WSIC is not electronically conductive but provides sufficient stable ionic conductivity for maintaining the EF reaction to work continuously, freeing it from liquid electrolyte cells and expensive ion exchange membranes, effectively enabling giant cathodic production of H_2O_2 without negative decomposition. The solid EF strategy uses only a simple cathodic flow cell to produce H_2O_2 and thus $OH^{\bullet}$ to decompose organic pollutants in a flowable aqueous or gaseous state, emerging as an exceptional EF for advanced applications.

RESULTS AND DISCUSSION

Conception of the solid EF strategy

Wood is a biological and sustainable material naturally composed of abundant, vertically aligned, top-down microchannels (e.g., lumens) (Figure 1A), which generally facilitates transport of O_2, water, and ions during the metabolism process. The unique porous structure of wood is used as a basis for constructing 3D porous architectural art within the connected microchannels, ideally suited for high ionic and electric conductors.[26–28] Here we used a simple and cost-effective way to fabricate a WSIC via a two-step strategy of initial photo-polymerization and a freeze-drying process (Figure 2A). Prior to the photo-polymerization process, natural wood chips were cut perpendicular to the growth direction of the tree (cross-section with a 16 cm^2 area) and immersed in an aqueous $LiNO_3$-agar/acrylamide ($LiNO_3$-agar/AM) mixture to enable its sufficient infiltration across the abundant microchannels. The following photo-polymerization was carried out by exposing it to UV light at 365-nm wavelength for a rapid curing process.

Inspired by ion and water molecular transport in trees, the WSIC in this work is designed to obtain promising ionic conduction by continuously capturing water molecules in the ambient environment resulting from the strong hygroscopicity of

Please cite this article in press as: Cui et al., Natural wood-derived solid ionic conductor for solid electro-Fenton strategy, Cell Reports Physical Science (2022), https://doi.org/10.1016/j.xcrp.2022.100857

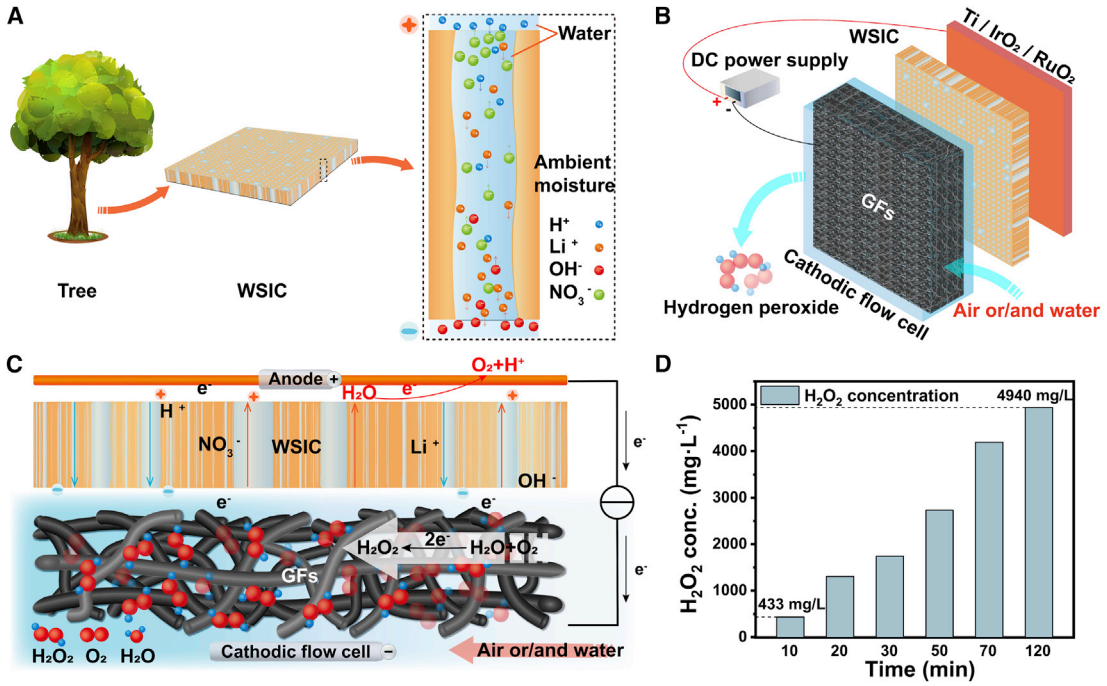

Figure 1. The solid EF strategy for cathodic production of H_2O_2

(A) Schematic of the WSIC directly processed from natural wood. In the EF reaction, the directional H^+, Li^+, OH^-, and NO_3^- migrate between the cathodic flow cell (filled with porous untreated GF) and the anode ($Ti/IrO_2/RuO_2$ electrode) to maintain a continuous EF reaction.

(B) The WSIC keeps the separated cathodic flow cell and anode working together to form a solid EF reactor.

(C) Schematic of flowable cathodic production of H_2O_2 using only natural H_2O and air.

(D) The tendency of accumulated H_2O_2 concentration generated in wet GF. Conditions for H_2O_2 accumulation: only with an air inflow rate of 0.8 L min^{-1} and current strength of 100 mA.

$LiNO_3$, which facilitates efficient ionization of $LiNO_3$ into Li^+ and NO_3^- charges that can directionally migrate along vertically aligned microchannels. Formation of continuous neighboring aqueous salt electrolytes in the abundant microchannels accelerates the ionization of H_2O to generate H^+ and OH^- charge providers to meet the requirements of the cathodic flow cell and anode, respectively. Here, a unique 2D salt-polymeric ionic transport layer covers the inner wall of the vertically aligned, top-down microchannels in the WSIC, enabling formation of a diffuse electric double-layer interface that maintains high ionic transport efficiency for stable ionic conductivity.

As shown in Figure 1B, we designed a novel solid EF device composed of a $Ti/IrO_2/RuO_2$ anode and cathodic flow cell on each side, closely connected by the sandwiched WSIC. When starting the EF reaction, the air-water mixture continuously flows in via an inserted plastic pipe and rapidly diffuses throughout the whole cathodic flow cell (Figure S1). Then the gas-liquid-solid three-phase interface in the cathodic flow cell is generated to enhance the oxygen mass transfer efficiency.[29] The produced H_2O_2 flows out continuously from the opposite side for collection and measurements. The cathodic flow cell is filled completely with a 3D porous GF matrix for electrochemical production of H_2O_2 in which H^+ and O_2 are required for 2e-ORR. The $Ti/IrO_2/RuO_2$ anode oxidates H_2O to generate O_2 and H^+ providers for maintaining continuous cathodic production of H_2O_2. Stable continuous production of H_2O_2 under mild conditions is a prerequisite for cathodic generation of $OH^{\bullet}$. Compared with traditional EF processes, the use of the cathodic flow cell in the solid EF device in this work makes it easier to transport the H_2O-air mixture to flow

Please cite this article in press as: Cui et al., Natural wood-derived solid ionic conductor for solid electro-Fenton strategy, Cell Reports Physical Science (2022), https://doi.org/10.1016/j.xcrp.2022.100857

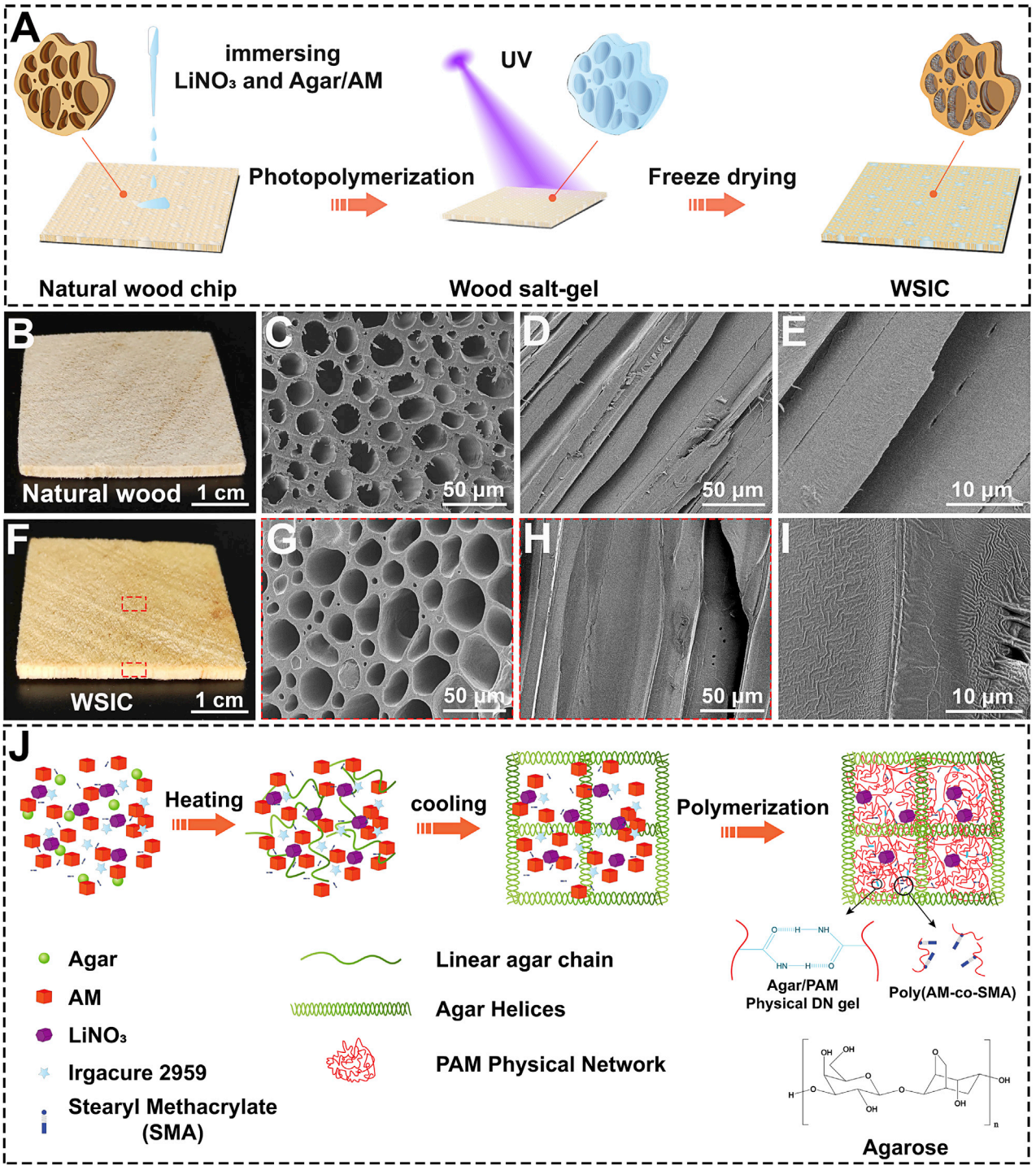

Figure 2. Fabrication and structure of the WSIC

(A) Schematic of fabrication of the WSIC using a two-step strategy. The balsa wood chip was cut perpendicular to the growth direction of the tree and directly immersed in an aqueous $LiNO_3$-agar/AM mixture to enable sufficient infiltration, followed by photo-polymerization to form double salt gels within the microchannels; a freeze-drying process was utilized to salting-out process for obtaining the WSIC.

(B and F) Picture of the natural wood and the WSIC sample at 1-cm scale.

(C and G) Cross-sectional scanning electron microscopy (SEM) image of the natural wood and the WSIC at 50-μm scale.

(D and H) Longitudinal sectional SEM image of the natural wood and the WSIC at 50-μm scale.

(E and I) Magnified longitudinal sectional SEM images of the surface of the natural wood and the WSIC at 10-μm scale.

(J) Schematic synthesis of double-network salt gels within the microchannels using a photo-polymerization strategy.

Please cite this article in press as: Cui et al., Natural wood-derived solid ionic conductor for solid electro-Fenton strategy, Cell Reports Physical Science (2022), https://doi.org/10.1016/j.xcrp.2022.100857

throughout the porous GF matrix, which facilitates formation of a sufficient gas-liquid-solid three phase interface, leading to higher O_2 mass transfer and utilization efficiency. When the H_2O-air mixture flows continuously into the cathodic flow cell, the 2e-ORR for O_2 proceeds to produce H_2O_2 on the surface of the GF at a 100-mA current, attributed to the directional diffusion of mobile ions within the WSIC while maintaining electric conductivity across the solid EF device (Figure 1C). Corresponding with the water molecule adsorption and transport process in the WSIC, H^+, Li^+, OH^-, and NO_3^- ions dissociate from H_2O and $LiNO_3$ in the 2D salt-polymeric ionic transport layer. Specifically, this strategy still can produce high H_2O_2 concentrations even when air flows in only throughout the wet GF matrix in the cathodic flow cell (Figure 1D). For example, H_2O_2 production increased markedly with an increase in time, from an initial 433.1 mg L^{-1} at 10 min up to the giant 4,939.6 mg L^{-1} at 120 min; the enhancement was associated with efficient accumulation of H_2O_2 without negative secondary degradation because of the closely separated anode on the other side by the WSIC. The highly hygroscopic WSIC captures and holds water molecules to continuously ionize H^+ for cathodic production of H_2O_2 via the 2e-ORR pathway. This makes it possible to decompose the flowable organic pollutants in an aqueous or gaseous state in the cathodic flow cell.

Characterization of the WSIC

As we can see in Figures 2B and 2C, natural balsa wood is composed of abundant, vertically aligned, top-down microchannels with a pore size of around 50 μm. It provides the basis for synthesis of the WSIC constructed with 3D double-network salt gels, which still generally retains the biological structure of natural wood (Figures 2A and 2J). The unique double-helix structure of double-network salt gels interwoven by agarose and polyacrylamide (PAM) chains is mechanically supported by a strong hydrogen bonding system. A freeze-drying process was utilized for the salting-out process, which enables collapse of 3D double-network salt gel around the inner walls to form a 2D salt-polymeric ionic transport layer as an ion charge provider across the microchannels (Figures 2G–2I). Unlike the original wood (Figures 2D and 2E), smooth plicated salt-polymeric layer profiles in the WSIC samples (Figures 2A and 2F) were clearly observed because of the synergistic aggregation effect resulting from the freeze-drying process.[30] However, the abovementioned treatments did not destroy the mechanical strength of wood; it still displayed a slight increase in compression modulus from 134 kPa to 150 kPa (Figure S2). Solid wood with high ionic conductivity is of great importance to make full use of natural wood as a stable ion transporter that enables formation of a "continuous aqueous salt bridge" for ion migration by capturing water molecules in ambient air. A WSIC made from natural wood has advantages of environmental compatibility, sustainability, eco-economy, and safety, with unique ion-conductive structures.

Electrochemical performances of the WSIC

The WSIC is of vital importance not only for rapid ionic transport for the EF reaction but also strictly separates the cathodic flow cell from the anode to form a solid EF device (Figure 1B). The electrochemical stability windows (ESWs) of the WSIC samples were determined to evaluate their ionic conduction ability under various conditions. The results showed that the WSIC operated stably at much wider voltages ranging from −0.88 to 3.20 V versus Ag/AgCl. Linear sweep voltammetry (LSV) measurements were used to determine the ESW of the WSIC with addition of 0.1, 1.0, 2.0, 3.0, and 4.0 M $LiNO_3$ concentration (Figure 3A), respectively. As expected, the ESW increased from 3.25 V (−0.77 to 2.64 V versus Ag/AgCl) to 3.77 V (−0.88 to 3.20 V versus Ag/AgCl), indicating that higher $LiNO_3$ concentration favors enhancement of ionic conductivity. For example, Tafel curves performed at different

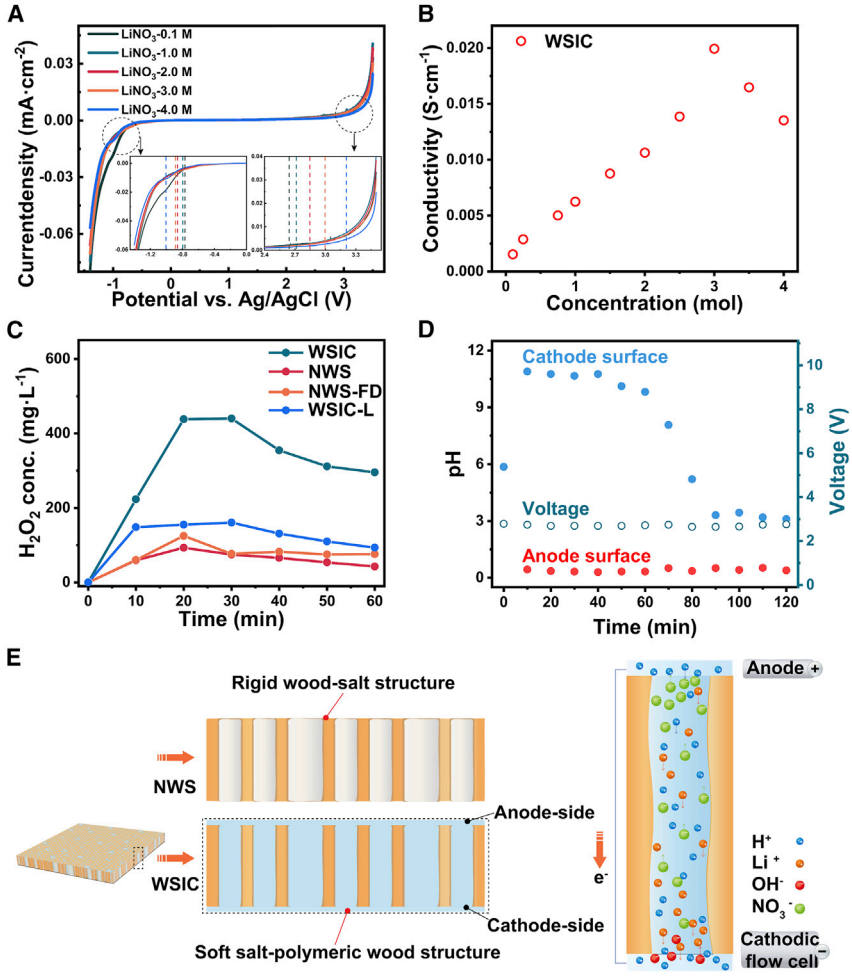

Figure 3. Electrochemical performances and working mechanism of the WSIC

(A) LSV curves of the WSIC with different $LiNO_3$ concentrations ranging from 0.1–4.0 M under the same scanning rate of 10 mV s^{-1}.

(B) Comparative ionic conductivity of the WSIC by utilizing different $LiNO_3$ concentrations.

(C) Comparative studies of H_2O_2 production in the cathodic flow cell of the solid EF device using four different samples: 1) WSIC; 2) natural wood chips cut parallel to the growth direction of the tree, followed by the same fabrication process as for the WSIC sample (WSIC-L); 3) natural wood chips the same as for the WSIC, directly immersed in aqueous 3.0 M $LiNO_3$ without any further treatment (NWS); and 4) samples the same as for the NWS expect for a supplemental freeze-drying process (NWS-FD). All testings were performed at 2.5 mm thickness, 16.0 cm^2 sample size, 100 mA current at pH 6.4, water flow rate of 66.4 mL h^{-1}, and air flux of 0.8 L min^{-1}.

(D) Determination of pH changes on the surface of the WSIC adjacent to the anode side and cathode side at 100 mA current and 0.8 L min^{-1} air flux.

(E) Schematic description of the mechanism of ion charge transport across the vertically aligned, top-down microchannels within the NWS and the WSIC.

$LiNO_3$ concentrations were derived from the highly polarized region of the corresponding LSV curves (Figure S3). It is noteworthy that the slope showed an initial increase and subsequent decrease tendency with a maximum of around 0.4050 V dec^{-1} at 3.0 M $LiNO_3$, attributed to the restriction of kinetics when increasing the salt concentration.[31]

According to the typical nanofluidics effect, the surface charge of the nano- or microchannel attracts counter-ions to transport while repelling the co-ions.[32] The building

Please cite this article in press as: Cui et al., Natural wood-derived solid ionic conductor for solid electro-Fenton strategy, Cell Reports Physical Science (2022), https://doi.org/10.1016/j.xcrp.2022.100857

electric field between the anode and cathode drives the directed migration of H^+, Li^+, OH^-, and NO_3^- ion charges along the continuous "aqueous salt bridge" across the abundant microchannels to form a closed circuit. In this process, the different ion charges migrate to guarantee the continuity of oxygen evolution reaction (OER) on the anode side and 2e-ORR on the cathodic flow cell side. The ionic conductivity of the WSIC mostly decides energy consumption and also the faradic efficiency. The results indicated that the ionic conductivity of the WSIC increased markedly up to a fairly high level of around 1.99×10^{-2} S cm^{-1} with addition of 3.0 M $LiNO_3$ and decreased when increasing its concentration to greater than 3.0 M (Figures 3B and S4A). The results demonstrated that moderate $LiNO_3$ addition can facilitate formation of a 2D salt-polymeric ionic transport layer and construction of an "continuous aqueous salt bridge" for promoting ion charge transport efficiency.

A thicker WSIC generally has a higher mechanical strength, but as a result, the resulting longer distance of the top-down WSIC restricts the efficiency of ion charge migration (Figures S4B and S5). The WSIC samples with a thickness ranging from 2.2–3.4 mm showed optimal ionic conductivity with a promising mechanical strength (Figures S2 and S5). Elegant approach to a 2D soft salt-polymeric layer around the inner wall of the open, vertically aligned microchannels contributes to the facile formation of a sufficient ionic transport pathway between the anode and cathode and avoids the major interface defect risks of rigid ion conductors without polymeric structure design (Figure 3E). H_2O_2 production was highly enhanced using the WSIC samples (cut perpendicular to the growth direction of the tree) ; however, it significantly decreased when the samples cut parallel to the growth direction of the tree (WSIC-L) were utilized under the same conditions (Figures 3C and S6). Compared with the WSIC samples, it only produced slight H_2O_2 with a nearly 4-fold decrease when empolying natural wood chips directly immersed in 3.0 M $LiNO_3$ followed by a freeze-drying process (NWS-FD) or natural wood chips directly immersed in 3.0 M $LiNO_3$ without any further treatment (NWS) (Figure 3C). The results showed that the NWS-FD samples with a higher ionic conductivity of 1.44×10^{-2} S cm^{-1} (Figures S7A and S7B) did not expectedly show more sufficient ionic transport across the anode and cathode, attributed to the lack of a soft ionic transport interface.

The voltage of the solid EF device markedly increased under a constant current of 100 mA when using the WSIC-L samples to work continuously for 20 min (Figure S8). The salt electrolyte of a typical $LiNO_3$ facilitates ionization of H^+ and OH^- from H_2O in an aqueous state, which provides a basis for sufficiently transporting H^+ to maintain ORR and OER to work stably on the cathode side and anode side, respectively. In the initial stage of the EF reaction, the 2e-OER on the anode side starts to decompose H_2O (from the WSIC) into O_2 and H^+, which diffuse across the WSIC to meet the requirement of the cathodic flow cell. With the EF reactions continued, H^+ first accumulates on the surface of the WSIC adjacent to the anode and subsequently migrates along the continuous salt-polymeric ionic transport structure to gradually replenish the exhausted ionized H^+ in the cathodic flow cell to generate H_2O_2. An important result in this regard was that the initial H_2O_2 production in the cathodic flow cell uses the H^+ directly ionized from the inflow H_2O but not that migrated from the anode side. This can be demonstrated in that the pH on the surface of the WSIC adjacent to the cathode side is shown to be nearly neutral in the initial state, but whereafter, increases rapidly with an alkalinity greater than 11.0 (Figure 3D). Each surface of the WSIC has an extremely different pH state during the initial EF reaction; for example, it shows strong acidity on the surface of the WSIC adjacent to the anode side but strong alkalinity on the cathode side. However, H^+

Please cite this article in press as: Cui et al., Natural wood-derived solid ionic conductor for solid electro-Fenton strategy, Cell Reports Physical Science (2022), https://doi.org/10.1016/j.xcrp.2022.100857

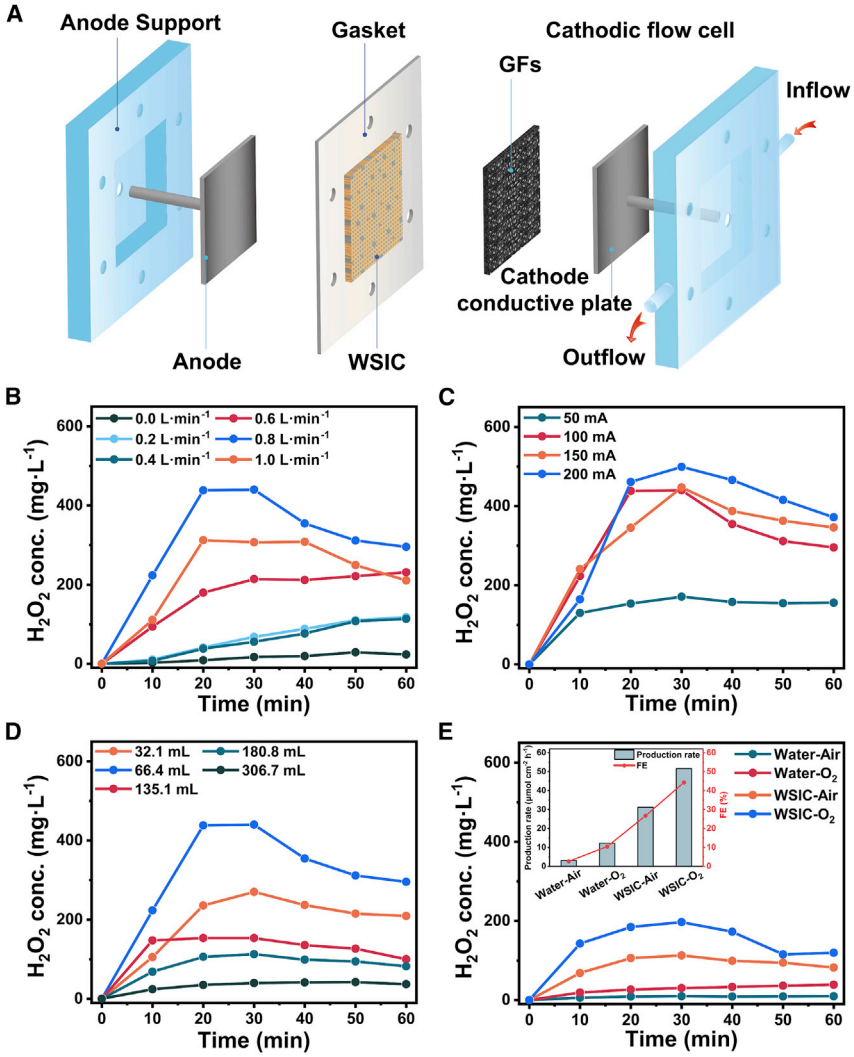

Figure 4. Production of H_2O_2 using the solid EF device

(A) Schematic illustration of the solid EF device design; all electrodes and the WSIC sample have the same area of 16 cm^2. The thickness of the WSIC sample is 2.5 mm.

(B–D) Determinations of H_2O_2 production in the cathodic flow cell under various conditions.

(B) Effects of air flux.

(C) Effects of current density.

(D) Effects of water flow rate.

(E) Comparative studies of immersed electrodes (for water-air and water-O_2) and the cathodic flow cell (for WSIC-air and WSIC-O_2) for H_2O_2 production; the inset case shows the comparative FE and production rate of H_2O_2. Conditions for H_2O_2 production were listed as follows: a fixed pH for water of 6.4, a fixed air flux of 0.8 L min^{-1} (C–E), a fixed current of 100 mA (B, D, and E). Experimental conditions for the immersed electrode were described as follows: pH 6.4, 180 mL aqueous $LiNO_3$ (for 100 mM concentration), and a fixed water flow rate of 66.4 mL h^{-1} (B and C) and 180.8 mL h^{-1} (E).

migrates across the WSIC from the anode side to the cathode side to neutralize the initial alkaline and even generate an acid environment after 60 min in the cathodic flow cell for a continuous EF reaction (Figures 3B and 3E).

Production of H_2O_2 via a solid EF device

In the electrochemical production of H_2O_2 using the solid EF apparatus as shown in Figure 4A, the anode and cathode separated by the sandwiched WSIC were essential

Please cite this article in press as: Cui et al., Natural wood-derived solid ionic conductor for solid electro-Fenton strategy, Cell Reports Physical Science (2022), https://doi.org/10.1016/j.xcrp.2022.100857

to allow the air-water mixture to flow only through the cathodic flow cell. For example, the use of an irregular WSIC sample with imprecise separation only produced much less H_2O_2 with 93.8 mg L^{-1} at 30 min, a 4.7-fold decrease compared with the regular WSIC sample (Figure S9). It was found that less H_2O_2 (around 8.9 mg L^{-1} at 20 min) was generated with only inflowing pure water without any air, demonstrating that the O_2 produced from the anode side does not sufficiently diffuse across the WSIC for the EF reaction because of the WSIC separation between the anode and cathode. Increasing air flux can undoubtedly enhance the mass transfer efficiency of O_2 and thus significantly enhance production of H_2O_2 to a maximum of 438.3 mg L^{-1} when using 0.8 L min^{-1} air flux (Figure 4B). However, much higher air flux of about 1.0 L min^{-1} resulted in dramatically decreased H_2O_2 production because of the lack of sufficient contact time for the gas-liquid-solid state.[33] To investigate the current dependence of the EF reaction, we recorded H_2O_2 generation for a longer time under different applied currents varying from 50 mA to 200 mA by maintaining an air and water flow velocity of 0.8 L min^{-1} and 66.4 mL h^{-1}, respectively (Figures 4B and 4C). The results indicated that the generated H_2O_2 concentration markedly increased with the increase in current; for example, a higher 461.0 mg L^{-1} H_2O_2 was produced at 200 mA, whereas it only generated a slight 153.7 mg L^{-1} at 50 mA at the same time of 20 min (Figure 4C). This further demonstrated that the employing current can effectively enhance H_2O_2 generation by expediting the conversion efficiency of O_2 in air to H_2O_2. However, a similar tendency of H_2O_2 generation with slight changes was observed when increasing the current to 150 and 200 mA, making the lower current of 100 mA acceptable for our solid EF device, with low energy consumption and cost effectiveness.

When water rapidly flows across the cathodic flow cell, H_2O_2 is electrochemically produced on the surface of the porous GF matrix with the introduced O_2 in air and ionized H^+ via the 2e-ORR pathway. Increasing the water flow rate decreased the generation efficiency of O_2 and H^+, which restrains the production efficiency of H_2O_2. Decreasing the water flow rate to 66.4 mL h^{-1} generated much more H_2O_2 of around 438.3 mg L^{-1} (Figure 4D). However, it is better to produce much less 220.2 mg L^{-1} H_2O_2 using a decreased water flow rate of 32.1 mL h^{-1} because of the negative decomposition of H_2O_2 in the alkaline cathodic flow cell. Previous studies have reported that H_2O_2 can be decomposed into hydrogen peroxide anions (HOO^-) at high alkalinity (pH > 11.0) and further converted to $OH^{\bullet}$ and $^{\bullet}O_2^-$ by Equations 4 and 5.[34,35] These results showed that H_2O_2 generation can be modulated by adjusting water flow velocity to meet different requirements.

$$H_2O_2 + HO^- \rightarrow HOO^- + H_2O \quad \text{(Equation 4)}$$

$$H_2O_2 + HOO^- \rightarrow OH^{\bullet} + {}^{\bullet}O_2^- + H_2O \quad \text{(Equation 5)}$$

Traditional submerged EF reactors provided an alternative route to produce H_2O_2 that avoided use of the anthraquinone oxidation process,[36] but still prevented the immersed electrode cells from practical application because of the unsatisfactory efficiency of H_2O_2 generation. In our solid EF device, use of the cathodic flow cell can markedly favor the formation of a sufficient gas-liquid-solid three-phase interface to enhance O_2 mass transfer through continuous inflow of the air-water mixture. Our solid EF yielded an approximately 7-fold increase in H_2O_2 production and faradic efficiency (FE) compared with a traditional submerged EF (for the immersed electrode) (Figure 4E). Although artificial addition of expensive pure O_2 into water can produce a higher H_2O_2 concentration, the fact that the cathodic flow cell still generates a satisfactory H_2O_2 with a promising FE when only using ambient air makes it more attractive and shows it to be superior to the traditional submerged EF when

Please cite this article in press as: Cui et al., Natural wood-derived solid ionic conductor for solid electro-Fenton strategy, Cell Reports Physical Science (2022), https://doi.org/10.1016/j.xcrp.2022.100857

ubiquitous air is used. The higher production rate of H_2O_2 in our solid EF device when only using air makes it a promising alternative for emerging a gaseous EF reaction, particularly in communities currently served by traditional aqueous EFs.

Bifunctional decomposition of aqueous and gaseous organic pollutants

H_2O_2 is a typical broad-spectrum clean oxidant that is promising for developing AOPs to decompose organic pollutants via the generated highly active $OH^{\bullet}$. In a cathodic flow cell, continuous in-site production of H_2O_2 facilitates generation of $^{\bullet}OH$ through a rapid catalytic activization process between H_2O_2 and the deposited Co[37,38] and Fe.[39] Iron oxychloride (FeOCl) is a typical layered metal chloride oxide that can rapidly switch between Fe(II) and Fe(III) when exposed to an electron acceptor or electron donor, and as a result, it can effectively activate H_2O_2 to produce $OH^{\bullet}$ over a wide pH range.[40,41] Here, we alloyed the cost-effective FeOCl catalyst onto the surface of GF using a simple approach (see Experimental procedures for synthesis details and Figure S10). The unique structures of iron atoms in the FeOCl compound favors efficient conversion between Fe (III) and Fe (II) when exposed to an electron acceptor or electron donor, as can be seen in Equations 6, 7, and 8.[40]

$$FeOCl + H_2O_2 \leftrightarrow Fe_{1-n}^{III}Fe_n^{II} + OOH^{\bullet} + H^+ \quad \text{(Equation 6)}$$

$$\equiv Fe^{II} + H_2O_2 \leftrightarrow \equiv Fe^{III} + OH^{\bullet} + OH^- \quad \text{(Equation 7)}$$

$$OH^{\bullet} + RhB \rightarrow oxidation\ \ products \quad \text{(Equation 8)}$$

A series of experiments for degradation of organic pollutants was carried out using a typical aqueous RhB mixture as the wastewater with 10.0 mg L^{-1} by modulating the wastewater flow velocity ranging from 43.5 to 341.0 mL h^{-1}. Pink aqueous RhB pollutants continuously flowed in through one side of the cathodic flow cell, and on the opposite side, the resulting colorless and transparent decomposition products rapidly flowed out with an outstanding stability and for a long period of time (Figures S11 and S12; Video S1). The above result showed that the solid EF device in this work has an attractive feature of in-site generation of $OH^{\bullet}$ for high-performance decomposition even when the organic wastewater flowed in with a high velocity of 341.0 mL h^{-1}. In particular, this strategy efficiently activates H_2O_2 to produce $OH^{\bullet}$ in a preferential acid environment. However, the presence of alkaline solutions generally favors dissolution of the active metal and also limits facile formation of $OH^{\bullet}$ because of the lack of a sufficient H^+ supply.

As can be seen in Figure 5A, the removal efficiency of typical rhodamine B (RhB) wastewater in an acidic environment (pH 3.0) rapidly increased to 84.4% in a very short time of 10 min with an inflow velocity of 43.5 mL h^{-1}. When maintaining the oxidation process for 180 min under the same inflow velocity, the removal efficiency further increased to 95.5%. To evaluate the decomposition ability, the inflow velocity was enhanced from 66.4 to 341.0 mL h^{-1}; the removal efficiency still steadily increased to achieve a much higher level of 99.9% when scaling up RhB pollutants. Supplemental acid addition to the reaction medium can suppress the sequential inactive metals and insufficient H^+ provider but result in a high production cost and also require further purification of the resulting by-products before discharge.

We also studied the possibility of decomposing organic RhB pollutants in a neutral state (pH 7.0) using an inflow velocity of 43.5 mL h^{-1}. The results indicated that the removal efficiency of RhB wastewater also rapidly increased to around 96.8% in a

Cell Reports
Physical Science
Article

CellPress
OPEN ACCESS

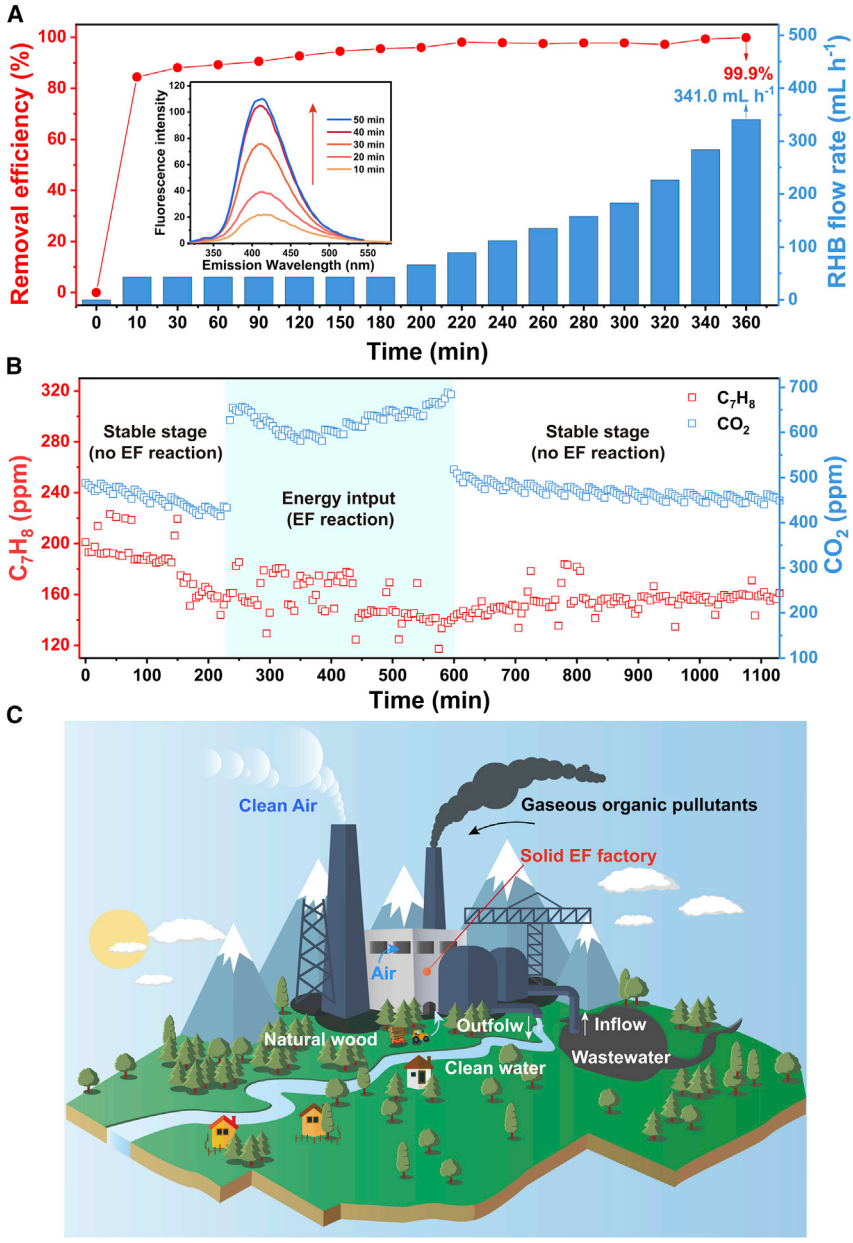

Figure 5. Solid EF strategy for bifunctional decomposition of aqueous and gaseous organic pollutants

(A) Determinations of the removal efficiency of the typical aqueous RhB mixture flowing through the cathodic flow cell filled completely with an FeOCl/GF matrix (RhB concentration of 10.0 mg L^{-1}) as a result of working time and RhB flow rate. The conditions were described as follows: a fixed pH for inflow water of around 2.0, a fixed air flux of 0.8 L min^{-1}, a fixed RhB flow rate of 43.5–341.0 mL h^{-1}, and a fixed current of 100 mA. The inset case showed experimental verification of $OH^{\cdot}$ generation at different times from 10–50 min.

(B) Experimental measurements of changes in high concentrations of gaseous toluene and CO_2 flowing through the cathodic flow cell in the solid EF device.

(C) Schematic illustration of the features of the solid EF strategy for efficiently degrading organic pollutants either in an aqueous or gaseous state, using only natural wood, water, and air.

Please cite this article in press as: Cui et al., Natural wood-derived solid ionic conductor for solid electro-Fenton strategy, Cell Reports Physical Science (2022), https://doi.org/10.1016/j.xcrp.2022.100857

short time of 10 min (Figure S13). A slight decrease to 76.1% at 60 min was observed because of formation of strong alkaline OH^- for decomposing H_2O_2 as well as the lack of a continuous H^+ supply. However, it then showed a significant increase up to higher than 90% when extending the reaction time, attributed to how the produced H^+ on the anode side migrates across the WSIC to change the alkaline environment in the cathodic flow cell, as demonstrated earlier (Figure 3D). Besides the RhB, other important organic pollutants of the typical tetracycline hydrochloride (TH) and p-nitrophenol (PNP) were also investigated with regard to their decomposition abilities using the solid EF device (Figure S14). The results also showed maximum removal rates of 84.6% and 79.9% at 50 and 110 min for TH and PNP, respectively, in a neutral environment, which verified the universal adaptability of our solid EF strategy for degradations of environmental organic pollutants.

The cathodic flow cell can be used to degrade not only wastewater but also exhibits enormous potential for decomposing gaseous organic pollutants as defined by the gaseous EF strategy. We had demonstrated that GF accumulated a much higher H_2O_2 concentration of 4,939.6 mg L^{-1} only by inflow air, making it possible to electrochemically generate $OH^{\bullet}$ for decomposing gaseous organic pollutants. The FeOCl/GF matrix in the cathodic flow cell was investigated by continuously flowing in gaseous stable toluene (C_7H_8) at room temperature. As shown in Figure 5B, the concentration of toluene and CO_2 without starting the gaseous EF reaction fluctuates initially around 180 $\pm$ 20 ppm and 425 $\pm$ 10 ppm, respectively. However, the concentration of toluene decreases to around 150 $\pm$ 20 ppm, whereas the concentration of CO_2 significantly increases to around 650 $\pm$ 50 ppm when the gaseous EF reaction starts to work. As the gaseous EF reaction stops, however, the concentrations of CO_2 and toluene sharply recover to the initial level with only slight changes. Compared with the initial concentration of toluene of 180 $\pm$ 20 ppm, a much lower concentration of toluene of about 46 $\pm$ 4 ppm was explored to find its corresponding decomposition behavior. A similar decreased level of the resulting toluene was around 30 ppm under initial higher or lower toluene concentration, although it showed a different variation curve of toluene and CO_2, attributed to the largely different initial toluene concentration (Figures 5B and S15). The higher production of CO_2 concentration using the much lower concentration of toluene of about 46 $\pm$ 4 ppm is observed. The results indicated that the direct oxidation of the GF was due to its leave uncovered structure, which is easier exposed to $OH^{\bullet}$. Relatively, the higher concentration of toluene at 180 $\pm$ 20 ppm facilitates its sufficient adsorption on the surface of GF and serves as a parclose to relieve the direct oxidation of the GF. The solid EF device opens up a new avenue for decomposition of volatile organic compounds (VOCs) at room temperature only using water, air, and natural wood.

The results demonstrated the superiority of our solid EF strategy featuring cathodic production of H_2O_2 as well as continuous degradation of organic pollutants in an gaseous or aqueous state, showing it to be eco-friendly, sustainable, and cost-efficient for upscaling practical applications. Compared with the exiting EF strategies, our solid EF strategy has the following advantages: (1) directly utilization of ubiquitous natural water, wood, and air without fossil fuel consumptions and an expensive proton exchange membrane; (2) eco-friendly cathodic production of H_2O_2 and $OH^{\bullet}$ for bifunctional decomposition of aqueous and gaseous organic pollutants; (3) only a requirement of mild conditions with room temperature and regular atmospheric pressure; (4) simplicity and cost-effectiveness for easier scale-up with flowable production of important H_2O_2 and $OH^{\bullet}$. It showed sustainability, industrial ecology, eco-efficiency, and green chemistry, which inevitably steer development of

next-generation of AOP technology for drinking water sterilization, industrial wastewater, and VOC purification.

In this work, we demonstrated a solid EF strategy for replacing conventional EF methods using a wood solid ionic conductor for flowable cathodic production of H_2O_2 and $OH^{\bullet}$ in gaseous or aqueous states. Cathodic generation of $OH^{\bullet}$ can continuously degrade aqueous organic pollutants (RhB, 99.9% removal efficiency) and also mineralize gaseous toluene to yield CO_2 and H_2O at room temperature. The fabricated solid EF device only uses natural water, wood, and air as regular input resources, overcoming the drawbacks of traditional EF strategies with intermittent H_2O_2 production, low efficiency, negative H_2O_2 decomposition, and use of immersed electrodes and proton exchange membranes. The comprehensive investigation of the WSIC made from natural wood resources demonstrated its superiority as a key material for a solid EF strategy with natural sustainability. The unique cathodic flowable decomposition of aqueous and gaseous organic pollutants exhibited a universal ability for developing next-generation of AOP technology. More detailed works will be performed to investigate the mechanism of degradation of organic pollutants and the physicochemical interaction as well as the competitive law between the GF, organic pollutants, and $OH^{\bullet}$ during the decomposition process.

EXPERIMENTAL PROCEDURES

Resource availability

Lead contact

Further information and requests for resources and reagents can be directed to the lead contact, D.L. (dtliu@scut.edu.cn).

Materials availability

This study did not generate new unique reagents.

Data and code availability

The authors declare that the data supporting the findings of this study are available within the article and the supplemental information. All other data are available from the lead contact upon reasonable request.

Materials and methods

Detailed materials and methods can be found in the supplemental experimental procedures.

SUPPLEMENTAL INFORMATION

Supplemental information can be found online at https://doi.org/10.1016/j.xcrp.2022.100857.

ACKNOWLEDGMENTS

This work was kindly supported by the Guangdong Basic and Applied Basic Research Foundation of Guangdong Province (2020A1515011013 and 2022A1515010910) and the Science and Technology Planning Project of Guangdong Province (2020A050515004). This work was also supported by the Science and Technology Development Fund from Macau SAR (FDCT) (0102/2019/A2, 0035/2019/AGJ, 0154/2019/A3, 0081/2019/AMJ, and 0033/2019/AMJ).

AUTHOR CONTRIBUTIONS

D.L. and H.P. conceived the project. J.C., Y.L., and C.L. synthesized the samples and performed SEM, compressive strength, production, and testing of H_2O_2 experiments. J.C., C.L., and Z.Q. measured the electrocatalytic performance and pollutant degradation ability. J.C. and D.L. wrote the manuscript. D.L. and H.P. discussed and revised the manuscript. All authors discussed the experimental results and revised the manuscript.

DECLARATION OF INTERESTS

The authors declare no competing interests.

Received: February 7, 2022
Revised: March 4, 2022
Accepted: March 23, 2022
Published: April 12, 2022

REFERENCES

1. Campos-Martin, J.M., Blanco-Brieva, G., and Fierro, J.L.G. (2006). Hydrogen peroxide synthesis: an outlook beyond the anthraquinone process. Angew. Chem. Int. Ed. *45*, 6962–6984. https://doi.org/10.1002/anie.200503779.

2. Brillas, E., Sirés, I., and Oturan, M.A. (2009). Electro-Fenton process and related electrochemical technologies based on Fenton's reaction chemistry. Chem. Rev. *109*, 6570–6631. https://doi.org/10.1021/cr900136g.

3. Matafonova, G., and Batoev, V. (2018). Recent advances in application of UV light-emitting diodes for degrading organic pollutants in water through advanced oxidation processes: a review. Water Rev. *132*, 177–189. https://doi.org/10.1016/j.watres.2017.12.079.

4. Liu, G., Ji, J., Huang, H., Xie, R., Feng, Q., Shu, Y., Zhan, Y., Fang, R., He, M., Liu, S., et al. (2017). UV/H_2O_2: an efficient aqueous advanced oxidation process for VOCs removal. Chem. Eng. J. *324*, 44–50. https://doi.org/10.1016/j.cej.2017.04.105.

5. Xu, J., Zheng, X., Feng, Z., Lu, Z., Zhang, Z., Huang, W., Li, Y., Vuckovic, D., Li, Y., Dai, S., et al. (2021). Organic wastewater treatment by a single-atom catalyst and electrolytically produced H_2O_2. Nat. Sustain. *4*, 233–241. https://doi.org/10.1038/s41893-020-00635-w.

6. Zhang, Y., Tang, Z.-R., Fu, X., and Xu, Y.J. (2010). TiO_2-Graphene nanocomposites for gas-phase photocatalytic degradation of volatile aromatic pollutant: is TiO_2-graphene truly different from other TiO_2-carbon composite materials? ACS Nano *4*, 7303–7314. https://doi.org/10.1021/nn1024219.

7. Zhang, F., Li, Y.H., Li, J.-Y., Tang, Z.-R., and Xu, Y.J. (2019). 3D graphene-based gel photocatalysts for environmental pollutants degradation. Environ. Pollut. *253*, 365–376. https://doi.org/10.1016/j.envpol.2019.06.089.

8. Teranishi, M., Hoshino, R., Naya, S.-I., and Tada, H. (2016). Gold-nanoparticle- loaded carbonate-modified titanium(IV) oxide surface: visible-light-driven formation of hydrogen peroxide from oxygen. Angew. Chem. Int. Ed. *55*, 12965–12969. https://doi.org/10.1002/ange.201606734.

9. Lu, Z., Chen, G., Siahrostami, S., Chen, Z., Liu, K., Xie, J., Liao, L., Wu, T., Lin, D., Liu, Y., et al. (2018). High-efficiency oxygen reduction to hydrogen peroxide catalysed by oxidized carbon materials. Nat. Catal. *1*, 156–162. https://doi.org/10.1038/s41929-017-0017-x.

10. Wang, N., Zheng, T., Zhang, G., and Wang, P. (2016). A review on Fenton-like processes for organic wastewater treatment. Chem. Eng. *4*, 762–787. https://doi.org/10.1016/j.jece.2015.12.016.

11. Brillas, E., and Garcia-Segura, S. (2020). Benchmarking recent advances and innovative technology approaches of Fenton, photo-Fenton, electro-Fenton, and related processes: a review on the relevance of phenol as model molecule. Sep. Purif. Technol. *237*, 116337. https://doi.org/10.1016/j.seppur.2019.116337.

12. Zhang, M.-h., Dong, H., Zhao, L., Wang, D.-x., and Meng, D. (2019). A review on Fenton process for organic wastewater treatment based on optimization perspective. Sci. Total Environ. *670*, 110–121. https://doi.org/10.1016/j.scitotenv.2019.03.180.

13. Yan, Q., Zhang, J., and Xing, M. (2020). Cocatalytic fenton reaction for pollutant control. Cell Rep. Phys. Sci. *1*, 100149–100153. https://doi.org/10.1016/j.xcrp.2020.100149.

14. Yan, Q., Lian, C., Huang, K., Liang, L., Yu, H., Yin, P., Zhang, J., and Xing, M. (2021). Constructing an acidic microenvironment by MoS_2 in heterogeneous fenton reaction for pollutant control. Angew. Chem. Int. Ed. *60*, 17155–17163. https://doi.org/10.1002/ange.202105736.

15. Viswanathan, V., Hansen, H.A., and Norskov, J.K. (2015). Selective electrochemical generation of hydrogen peroxide from water oxidation. Chem. Lett. *6*, 4224–4228. https://doi.org/10.1021/acs.jpclett.5b02178.

16. Oturan, M.A., and Aaron, J.-J. (2014). Advanced oxidation processes in water/wastewater treatment: principles and applications. A Review. Crit. Rev. Environ. Sci. Technol. *44*, 2577–2641. https://doi.org/10.1080/10643389.2013.829765.

17. Siahrostami, S., Li, G.-L., Viswanathan, V., and Norskov, J.K. (2017). One- or two-electron water oxidation, hydroxyl radical, or H_2O_2 evolution. J. Phys. Chem. Lett. *8*, 1157–1160. https://doi.org/10.1021/acs.jpclett.6b02924.

18. Ma, L., Zhou, M., Ren, G., Yang, W., and Liang, L. (2016). A highly energy-efficient flow-through electro-Fenton process for organic pollutants degradation. Electrochim. Acta *200*, 222–230. https://doi.org/10.1016/j.electacta.2016.03.181.

19. Yin, F., Liu, Y., Wang, C., and Liu, H. (2018). Assessing the electron transfer and oxygen mass transfer of the oxygen reduction reaction using a new electrode kinetic equation. Phys. Chem. Chem. Phys. *20*, 16159–16166. https://doi.org/10.1039/C8CP01305E.

20. Li, Z., Shen, C., Liu, Y., Ma, C., Li, F., Yang, B., Huang, M., Wang, Z., Dong, L., and Wolfgang, S. (2020). Carbon nanotube filter functionalized with iron oxychloride for flow-through electro-Fenton. Appl. Catal. B Environ. *260*, 118204. https://doi.org/10.1016/j.apcatb.2019.118204.

21. Tang, H., Zhu, Z., Shang, Q., Tang, Y., Zhang, D., Du, Y., Liu, M., Yin, K., and Liu, C. (2021). Highly efficient continuous-flow electro-fenton treatment of antibiotic wastewater using a double-cathode system. ACS Sustain. Chem. Eng. *9*, 1414–1422. https://doi.org/10.1021/acssuschemeng.0c08705.

22. Agladze, G.R., Tsurtsumia, G.S., Jung, B.I., Kim, J.S., and Gorelishvili, G. (2007). Comparative study of hydrogen peroxide electro-generation on gas-diffusion electrodes in undivided and membrane cells. J. Appl. Electrochem. *37*, 375–383. https://doi.org/10.1007/s10800-006-9269-x.

23. Chaudhuri, S.K., and Lovley, D.R. (2003). Electricity generation by direct oxidation of glucose in mediatorless microbial fuel cells. Nat. Biotechnol. *21*, 1229–1232. https://doi.org/10.1038/nbt867.

24. Kim, J.R., Jung, S.H., Regan, J.M., and Logan, B.E. (2007). Electricity generation and microbial community analysis of alcohol powered microbial fuel cells. Bioresour. Technol. *98*, 2568–2577. https://doi.org/10.1016/j.biortech.2006.09.036.

25. Zhang, W., Xi, J., Li, Z., Zhou, H., Liu, L., Wu, Z., and Qiu, X. (2013). Electrochemical activation of graphite felt electrode for VO^{2+}/VO_2^+ redox couple application. Electrochim. Acta *89*, 429–435. https://doi.org/10.1016/j.electacta.2012.11.072.

26. Zhu, M.W., Song, J.W., Li, T., Gong, A., Wang, Y.B., Dai, J.Q., Yao, Y.G., Luo, W., Henderson, D., and Hu, L.B. (2016). Highly anisotropic, highly transparent wood composites. Adv. Mater. *28*, 5181–5187. https://doi.org/10.1002/adma.201600427.

27. Parham, R.A., and Gray, R.L. (1984). The chemistry of solid wood. Advan. Chem. Ser. 3–56. https://doi.org/10.1021/ba-1984-0207.fw001.

28. Wu, Q.-Y., Wang, C., Wang, R., Chen, C., Gao, J., Dai, J., Liu, D., Lin, Z., and Hu, L. (2020). Salinity-gradient power generation with ionized wood membranes. Adv. Energy Mater. *10*, 1902590. https://doi.org/10.1002/aenm.201902590.

29. Zhang, Q., Zhou, M., Ren, G., Li, Y., Li, Y., and Du, X. (2020). Highly efficient electrosynthesis of hydrogen peroxide on a superhydrophobic three-phase interface by natural air diffusion. Nat. Commun. *11*, 1–11. https://doi.org/10.1038/s41467-020-15597-y.

30. Hua, M., Wu, S., Ma, Y., Zhao, Y., Chen, Z., Frenkel, I., Strzalka, J., Zhou, H., Zhu, X., and He, X. (2021). Strong tough hydrogels via the synergy of freeze-casting and salting out. Nature *590*, 594–599. https://doi.org/10.1038/s41586-021-03212-z.

31. Chen, S., Sun, P., Sun, B., Humphreys, J., Zou, P., Xie, K., and Tao, S. (2021). Nitrate-based 'oversaturated gel electrolyte' for high-voltage and high-stability aqueous lithium batteries. Energy Storage Mater. *37*, 598–608. https://doi.org/10.1016/j.ensm.2021.02.038.

32. Daiguji, H., Yang, P.D., and Majumdar, A. (2004). Ion transport in nanofluidic channels. Nano Lett. *4*, 137–142. https://doi.org/10.1021/nl0348185.

33. Li, D., Zheng, T., Liu, Y., Hou, D., Yao, K.K., Zhang, W., Song, H., He, H., Shi, W., Wang, L., and Ma, J. (2020). A novel Electro-Fenton process characterized by aeration from inside a graphite felt electrode with enhanced electrogeneration of H_2O_2 and cycle of Fe^{3+}/Fe^{2+}. J. Hazard. Mater. *396*, 122591–122601. https://doi.org/10.1016/j.jhazmat.2020.122591.

34. Sun, R.C., Tomkinson, J., Ma, P.L., and Liang, S.F. (2000). Comparative study of hemicelluloses from rice straw by alkali and hydrogen peroxide treatments. Carbohydr. Polym. *42*, 111–122. https://doi.org/10.1016/S0144-8617(99)00136-8.

35. Wang, H., Bian, Z.Y., and Sun, D.Z. (2011). Degradation mechanism of 4- chlorophenol with electrogenerated hydrogen peroxide on a Pd/C gas-diffusion electrode. Water Sci. Technol. *63*, 484–490. https://doi.org/10.2166/wst.2011.247.

36. Yi, Y.H., Wang, L., Li, G., and Guo, H.C. (2016). A review on research progress in the direct synthesis of hydrogen peroxide from hydrogen and oxygen: noble-metal catalytic method, fuel-cell method and plasma method. Catal. Sci. Technol. *6*, 1593–1610. https://doi.org/10.1039/C5CY01567G.

37. Guo, X.X., Hu, T.T., Meng, B., Sun, Y., and Han, Y.F. (2020). Catalytic degradation of anthraquinones-containing H_2O_2 production effluent over layered Co-Cu hydroxides: defects facilitating hydroxyl radicals generation. Appl. Catal. B Environ. *260*, 118157–118166. https://doi.org/10.1016/j.apcatb.2019.118157.

38. Chen, Y.-H., Qi, M.Y., Li, Y.H., Tang, Z.R., Wang, T., Gong, J., and Xu, Y.J. (2021). Activating two-dimensional Ti_3C_2Tx-MXene with single-atom cobalt for efficient CO_2 photoreduction. Cell Rep. Phys. Sci. *2*, 100371–100384. https://doi.org/10.1016/j.xcrp.2021.100371.

39. Cao, P., Quan, X., Zhao, K., Chen, S., Yu, H., and Niu, J. (2020). Selective electrochemical H_2O_2 generation and activation on a bifunctional catalyst for heterogeneous electro-Fenton catalysis. J. Hazard. Mater. *382*, 121102–121110. https://doi.org/10.1016/j.jhazmat.2019.121102.

40. Yang, X.-j., Xu, X.-m., Xu, J., and Han, Y.-f. (2013). Iron oxychloride (FeOCl): an efficient fenton-like catalyst for producing hydroxyl radicals in degradation of organic contaminants. J. Am. Chem. Soc. *135*, 16058–16061. https://doi.org/10.1021/ja409130c.

41. Sun, M., Chu, C., Geng, F., Lu, X., Qu, J., Crittenden, J., Elimelech, M., and Kim, J.-H. (2018). Reinventing fenton chemistry: iron oxychloride nanosheet for pH-insensitive H_2O_2 activation. Environ. Sci. Technol. Lett. *5*, 186–191. https://doi.org/10.1021/acs.estlett.8b00065.